Original Article

Characteristics of axisymmetric viscous incompressible flow passing a torus rotating about its centerline

Pairin Suwannasri*

Department of Mathematics, Statistics and Computer, Faculty of Science,
Ubon Ratchathani University, Warin Chamrap, Ubon Ratchathani, 34190 Thailand.

Abstract

The present numerically investigates the axisymmetric flow past a rotating torus in a viscous incompressible fluid. The surface of the torus rotates with constant velocity around its centerline. A numerical model has been developed for the governing equation in the toroidal coordinate system. The rotating boundary of a torus generates inertia in the surrounding fluid. There are two interesting regimes. In one of them, a rotation of torus surface generates a toroidal fluid region which envelopes the torus. In another one a rotation of torus surface generates the jet of fluid expelled from the hole downward. We focus on the hydrodynamics of a torus effected by a rotational rate (α) and the aspect ratios (Ar). The numerical simulations are performed for three aspect ratios, Ar = 2, 3 and 5, where Ar is defined as ratio of torus radius (b) to cross-section radius of torus (a) and the range of rotational rate $-4.0 \leq \alpha \leq 2.0$, where α is defined as ratio of tangential tank-treading motion of torus surface to the uniform far-field velocity.

Keywords: axisymmetric flow, toroidal coordinate system, rotating torus

1. Introduction

There are a number of basic flows that have received great attention from engineers, such as flat plate boundary layer flow, backward-facing step flow, flows around bluff bodies (sphere, cylinder, aeroplane wings, etc.), and others. The torus as a bluff body has attractive features of behaving like the sphere at small aspect ratio, and locally like the circular cylinder at large aspect ratios. The torus (or ring) with its axis of symmetry placed parallel to the flow can be considered as a bluff-body geometry that spans the flow patterns shown by the sphere and circular cylinder as a single geometric parameter is varied. The flow around a torus has not been investigated widely in the literature.

The Stokes flow over a torus of anchor ring type has been studied for the two axisymmetric flows which occur when either the torus rotates about its axis of symmetry in an unbounded quiescent fluid or when the torus is at rest in a uniform stream directed along its axis of symmetry. The first attempt to solving this problem was made by Ghosh (1927). However, his solution is unacceptable physically since it leads to a discontinuity in pressure over the plane of symmetry of the hole. Pell and Payne (1960) made a detailed study of the problem and correctly treated the value taken by the stream function vanishes on the body as one of the unknowns of the problem. Majumdar and O'Neill (1977) presented an alternative solution of this problem that it provides the solution in a particularly simple form compared with that given by Pell and Payne.

In an extensive work on the hydrodynamics of a torus, Jonhson and Wu (1979) studied the flow around a torus for five different situations: Translation along the longitudinal axis, translation along the two transverse axes, rotation along. However, they did not address the problem of rotation around the centerline. There are very few studies that discussed this problem.

* Corresponding author.
 Email address: pairin_77@hotmail.com

It is known, that a torus rotates about its centerline with a constant velocity in a surrounding fluid. The hydrodynamics of a rotating torus is interesting for two reasons: firstly, most stiff or semiflexible ring polymers, e.g. DNA miniplasmids are modeled as a torus, and secondly, it has a simple geometry, which can be describe as a self-propelled organism. Thaokar *et al.* (2007) studied the hydrodynamics of a torus rotating about its centerline and the motion of torus along a cylindrical track which can describe self-propelled microorganisms. They obtained the analytical and numerical solutions of the Stoke flow passing a rotating torus. Leshansky and Kenneth (2008) studied the smoking ring propulsion technique, originally proposed by Purcell in 1930 for self-locomotion at low Reynolds number (Stokes flows). They considered self-locomotion of a torus swimmer powered by surface rotation.

In some sense this paper extends the studies of Thaokar *et al.* and Leshansky and Kenneth towards finite Reynolds numbers. The objective of the present work is to understand the corresponding underlying mechanism of axisymmetric flow past a torus rotating about its centerline for moderate Reynolds number. The problem of rigid torus motion in a viscous liquid is formulated then recast as fluid flow past a rotating torus in terms of the toroidal coordinate system by a linear change of variables. A short description of a numerical algorithm based on a projection method for solving the Navier-Stokes equations follows, and finally the results of various numerical experiments are reported and discussed.

2. Problem Formulation and Governing Equations

A rigid open torus, with a cross-sectional radius a, torus radius b, and surface S_b is placed axisymmetrically in a uniform stream which flows with constant velocity U_∞ and pressure p_∞. A sketch of the geometry is illustrated in Figure 1. In order to study the fluid flow passing a torus, we introduce the toroidal coordinates, where the coordinate surface fit the surface of the torus boundary. In terms of the toroidal coordinates and the assumption of axisymmetry, the governing Navier-Stokes equations in dimensionless form are given by

$$\frac{\partial v_\xi}{\partial t} + \frac{1}{h}\left(v_\xi \frac{\partial v_\xi}{\partial \xi} + v_\eta \frac{\partial v_\xi}{\partial \eta}\right) + \frac{1}{c}\left(v_\eta^2 \sin\xi - v_\xi v_\eta \sinh\eta\right) =$$

$$-\frac{1}{h}\frac{\partial p}{\partial \xi} + \frac{2}{Re}\left[\frac{1}{h^2}\left(\frac{\partial^2 v_\xi}{\partial \xi^2} + \frac{\partial^2 v_\xi}{\partial \eta^2}\right)\right.$$

$$-\frac{1}{ch}\left(\sin\xi \frac{\partial v_\xi}{\partial \xi} + 2\sinh\eta \frac{\partial v_\eta}{\partial \xi} - 2\sin\xi \frac{\partial v_\eta}{\partial \eta}\right)$$

$$+\left(\frac{\coth\eta}{h^2} - \frac{1}{ch}\sinh\eta\right)\frac{\partial v_\xi}{\partial \eta} + \frac{1}{c^2}\left(\cosh\eta \cos\xi - 1\right)v_\xi$$

$$+\left(\frac{1}{ch}\cosh\eta - \frac{2}{c^2}\left(\sin^2\xi + \sinh^2\eta\right)\right)v_\xi$$

$$+\left(\frac{\sin\xi}{c^2 \sinh\eta}\left(\left(2 - 2\cosh\eta\cos\xi\right) + \sinh^2\eta\right) + \sinh^2\eta\right)v_\eta\right]$$

$$(2)$$

$$\frac{\partial v_\eta}{\partial t} + \frac{1}{h}\left(v_\xi \frac{\partial v_\eta}{\partial \xi} + v_\eta \frac{\partial v_\eta}{\partial \eta}\right) + \frac{1}{c}\left(v_\xi^2 \sinh\eta - v_\xi v_\eta \sin\xi\right) =$$

$$-\frac{1}{h}\frac{\partial p}{\partial \eta} + \frac{2}{Re}\left[\frac{1}{h^2}\left(\frac{\partial^2 v_\eta}{\partial \xi^2} + \frac{\partial^2 v_\eta}{\partial \eta^2}\right)\right.$$

$$-\frac{1}{ch}\left(\sin\xi \frac{\partial v_\eta}{\partial \xi} - 2\sinh\eta \frac{\partial v_\xi}{\partial \xi} + 2\sin\xi \frac{\partial v_\xi}{\partial \eta}\right)$$

$$+\left(\frac{\coth\eta}{h^2} - \frac{\sinh\eta}{ch}\right)\frac{\partial v_\eta}{\partial \eta} - \frac{\sin\xi \sinh\eta}{c^2}v_\xi$$

$$+\left(\frac{\cosh\eta}{ch} - \frac{2}{c^2}\left(\sin^2\xi + \sinh^2\eta\right)\right)v_\eta$$

$$+\frac{1}{c^2}\left(\sin^2\xi + \left(\cosh\eta \cos\xi - 1\right) + \frac{\left(1 - \cosh\eta\cos\xi\right)^2}{\sinh^2\eta}\right)v_\eta\right]$$

$$(3)$$

$$\frac{1}{h}\left(\frac{\partial v_\xi}{\partial \xi} + \frac{\partial v_\eta}{\partial \eta}\right) - \frac{2h\sin\xi}{c}v_\xi + \left(\coth\eta - \frac{2h\sinh\eta}{c}\right)v_\eta = 0,$$

$$(4)$$

where p is the pressure, v_ξ and v_η are the velocity components in ξ and η directions, respectively, and $h = c/\left(\cosh\eta - \cos\xi\right)$. The velocities are non dimensionalized with the free stream velocity, U_∞, all lengths are non dimensionalized with the radius a and the pressure by ρU_∞^2. Here, denotes the Reynolds number defined by $Re = \frac{2U_\infty a}{v}$, where v is the kinematic viscosity coefficient. Boundary conditions for v_ξ and v_η include the no-slip and impermeability conditions

$$v_\xi = \alpha, \ v_\eta = 0, \ \xi \in (0, 2\pi], \eta = \eta_0, \quad (5)$$

where $\alpha = (a\omega)/U_\infty$ is the nondimensional rotational velocity at the surface, the periodicity conditions

$$(\xi, \eta) = v_\xi\left(\xi + 2\pi, \eta\right), \ v_\eta\left(\xi, \eta\right) =$$

$$v_\eta\left(\xi + 2\pi, \eta\right), \ p\left(\xi, \eta\right) = p\left(\xi + 2\pi, \eta\right). \quad (6)$$

and the far-field condition

$$\vec{v} = \left(v_r, v_z\right) = \left(0, 1\right), \ p = \frac{p_\infty}{\rho U_\infty^2} \text{ as } r^2 + z^2 \to \infty. \quad (7)$$

Here, v_r are v_z the components of the velocity vector in the cylindrical coordinate system with

$$v_{\xi} = \left(-\frac{h}{a}\sinh\eta\sin\xi \right)v_r + \left(\frac{h}{a}\left(\cosh\eta\cos\xi - 1\right) \right)v_z,$$

$$v_{\eta} = \left(-\frac{h}{a}\left(\cosh\eta\cos\xi - 1\right) \right)v_r - \left(\frac{h}{a}\sinh\eta\sin\xi \right)v_z. \quad (8)$$

On the axis of symmetry at $r = 0$ the velocity components and pressure satisfy the following conditions

$$\frac{\partial v_{\xi}}{\partial \eta} = 0, v_{\eta} = 0 \text{ and } \frac{\partial p}{\partial \eta} = 0. \quad (9)$$

The two most important hydrodynamic characteristics of the flow around the body are the net force and angular momentum. The net force is decomposed into components F_L and F_D perpendicular and parallel to the flow direction. The net torque and F_L are equal to zero due to the symmetry of the flow. The drag coefficient is defined as, $C_D = \dfrac{F_D}{0.5\rho A_{frontal}U_{\infty}^2}$,

where ρ and $A_{frontal}$ are the fluid density and the projected frontal area of the body, respectively. The drag coefficient comprises a pressure drag coefficient and a viscous drag coefficient, i.e. $C_D = C_{D_p} + C_{D_f}$. They are defined as

$$C_{D_p} = -\frac{\sinh^2\eta_0}{b}\int_0^{2\pi} p\frac{\sin\xi}{\left(\cosh\eta_0 - \cos\xi\right)}h^2 d\xi, C_{D_f}$$

$$= -\frac{\sinh^2\eta_0}{b}\int_0^{2\pi} \frac{2\omega\left(\cosh\eta_0 - 1\right)}{Re\left(\cosh\eta_0 - \cos\xi\right)}hd\xi. \quad (10)$$

The vorticity ω is defined by the following equation

$$\omega = \frac{1}{h^3\sinh\eta_0}\left(\frac{\partial}{\partial\xi}\left(hv_{\eta}\right) - \frac{\partial}{\partial\eta}\left(hv_{\xi}\right) \right). \quad (11)$$

3. Numerical Methods

In the case of steady flow, time in Equation (2) and (3) can be considered as an artificial (iterative) parameter. A staggered arrangement of the variables on a uniform grid is used. A two-step time-split projection method is utilized to advance the flow field. First, the velocity components are advanced from time level "n" to an intermediate level "*" by solving Equation (2) and (3) explicitly without the pressure term. In the advection-diffusion step, the spatial derivatives are approximated by the central finite differences. One side finite differences are utilized near boundaries due to the staggered arrangement of variables. Then the Poisson equation for the pressure is solved fully implicitly by the method of stabilizing correction (Yanenko, 1971). The equation for pressure is derived by using the mass conservation requirement for each computational cell. Once the pressure is

updated, the final level is computed with a pressure-correction step. Far-field boundary conditions (7) are shifted on the boundary of domains Ω_1 and Ω_2 which are defined as

$$\Omega_1 = \left\{ \left(\xi,\eta\right) \mid 0 \le \xi \le \varepsilon_{\xi}, 0 \le \eta \le \varepsilon_{\eta} \right\},$$

$$\Omega_2 = \left\{ \left(\xi,\eta\right) \mid 2\pi - \varepsilon_{\xi} \le \xi \le 2\pi, 0 \le \eta \le \varepsilon_{\eta} \right\}, \quad (12)$$

where $\varepsilon_{\eta} = K\Delta_{\eta}$ and $\varepsilon_{\xi} = M\Delta_{\xi}$, K and M are integer numbers, Δ_{η} and Δ_{ξ} are the size of computational cell in the η and ξ directions, respectively.

The grid refinement test has been carried out for the two Reynolds numbers Re = 20 and 40 and the three aspect ratios Ar = 2, 3 and 5. Three grids with refinement factor $h_{coarse}/h_{fine} = 1.5$ are used. The second validation is performed for the flow around a steady torus (torus surface does not move). The largest difference, about 10%, is observed in C_{D_p} and C_{D_f} for Re = 20 and Ar = 2. Nevertheless, the agreement between total drag coefficients remains reasonable.

There are no previous numerical or experimental results for the incompressible fluid flow past a torus rotating about its centerline. In order to validate the computational code, we developed the numerical code for flow past two rotating circular cylinders. We expected that the results of flow over a rotating torus at large are similar to the results of flow over two rotating circular cylinders with large gap spacing between the cylinder surfaces. Our assumption was made on the basis that for large aspect ratio the characteristics of flow over a non-rotating torus are locally similar to the characteristics of flow over a non-rotating circular cylinder (Sheard et al., 2005).

4. Results and Discussion

The characteristics of flow passing a rotating torus at the Reynolds number Re = 40 with a rate of rotation of $-4.0 \le \alpha \le 2.0$ for a variety of aspect rations were studied. The torus is placed in a stream (from down to up) of uniform speed as shown in Figure 1. The positive direction of angular velocity of torus surface $\alpha > 0$, denoted as α^+, is such that on the inner ring surface, the rotational velocity of the wall is opposed to the oncoming flow direction.
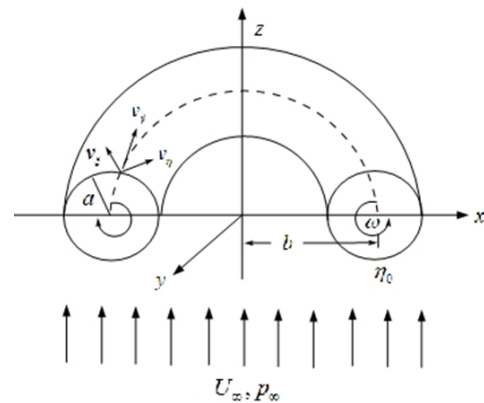

Figure 1. Sketch of the geometry of the torus.

4.1 Flow patterns

We first show in Figure 2 the visualization of flow patterns and the directions of velocity vector for the case Ar = 2, Re = 40 with a sequence of rotation rates $-3.5 \leq \alpha \leq 2.0$. For $\alpha = 0$, non-rotating torus, the fluid passes through the hole in the torus on the axis developing a detached torodial bubble on the axis downstream of the torus resulting in two stagnation points on the symmetry axis $(r = 0)$. Rotation of surface results of formation a fluid region which envelopes the torus. Rotation in positive direction results that detached vortex disappear. For $0 < \alpha < 1.0$, the incoming free stream main flow separates into the two parts: one passing through the hole in the torus above "enveloping zone" and the other moving downward and around the "enveloping zone". As α^{+} increases, a larger amount of fluid is involved in the rotation and the main stream cannot longer pass through the hole of rigid torus (Figure 2 (b2)). The main stream flows around the rotating toroidal fluid region which encloses the rigid torus rotating around its centerline.

Figure 2 (a1)-(a3) demonstrate streamline pattern for negative rotation denoted as α^{-}. The rotating surface accelerated portion of the incoming stream passing through the hole and generates the jet of fluid expelled from the hole downward. This jet pushes the detached vortex babble "A" in the downstream direction, see Figure 2 (a1) and (a2). At the same time vortex "A" is extended in the upstream direction and splits by two "A" and "A'''". When the absolute value of α^{-} increases this jet separates from the axis of symmetry of the detached vortex babble, see Figure 2 (a3). The front stagnation point separates the main stream into three parts; one passing and accelerating in the hole, the second one flowing downward and around the toroidal vortex zone "A",

and the other one turning back in the upstream direction by toroidal vortex zone "A" going around "enveloping zone" and expelled in the main stream through the hole in the torus.

4.2 Flow quantities

The pressure and vorticity distributions on the torus surface for Re = 40 are depicted on Figures 3 and 4. In Figures 3 and 4, the circumferential direction θ varies from 0° to 360° and corresponds to the angular coordinate of the circular cross-section of the torus by meridional plane. The outer surface of the torus corresponds to $0° \leq \theta \leq 180°$ and the inner surface corresponds to $180° \leq \theta \leq 360°$.

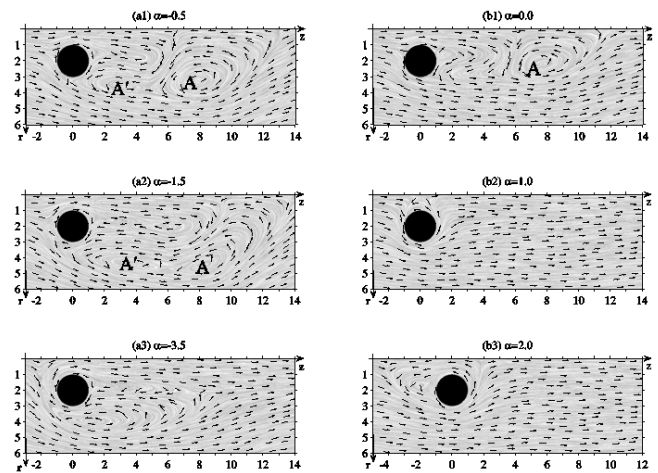Figure 3 shows the pressure on the outer surface of torus decreases due to the flow is accelerated by the rotation.

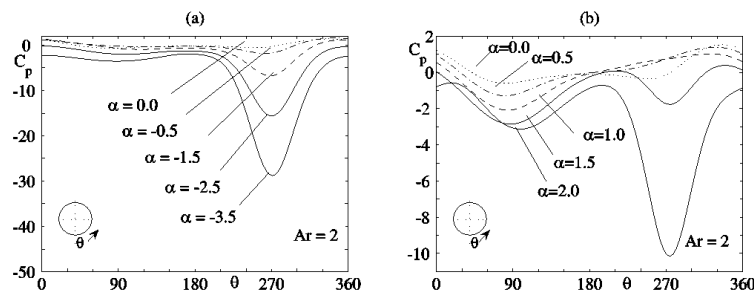Figure 2. Streamline patterns of flow past a revolving torus at Re = 40 with Ar = 2.

Figure 3. Influence of the rotation speed α on the surface pressure coefficient in the circular cross-section by meridional plane for Re = 40
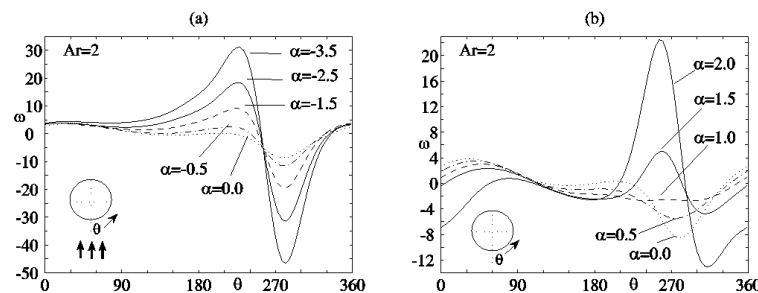

Figure 4. Influence of the rotation speed α on the surface vorticity in the circular cross-section by meridional plane for Re = 40.

At the inner surface of torus, the pressure is higher than at the outer, except that the minimum peak appears at $\theta = 270°$ for Ar = 2 and $\alpha = 2.0$. For a negative rotation α^-, the pressure on the inner surface of torus where the flow is accelerated decreases monotonically as increases $|\alpha^-|$. There is a minimum point at $\theta = 270°$. As absolute value of α^- increases, the local peak becomes sharper.

Figure 4 shows the vorticity distribution on the torus surface for different rotational speeds at Ar = 2. In the case of $\alpha = 0$, the vorticity have two positive and negative peaks at $\theta \approx 40°$ and $\theta \approx 290°$, respectively. As α^+ increases, the positive peak decreases roughly at the same location on the outer surface of the torus as shown in Figure 4 (b). The changes in the variation of surface vorticity on the rotational speed are more serve on the inner surface. As α^+ increases, the value of negative peak at $\theta \approx 290°$ decreases and becomes to one local positive and two local negative peaks for large aspect ratio. For a negative rotation, the changes of voticity on the rotational speed are more serve on the inner surface of the torus as shown in Figure 4 (a). On the inner surface, as $|\alpha^-|$ increases, the value of positive local peak at $\theta \approx 210°$ increases, while the value of negative local peak at $\theta \approx 290°$ is decreasing with almost the same in magnitude.

4.3 Drag coefficients

The variations of drag coefficient C_D with rate of rotation for the three aspect ratios at Re = 40 are shown in Figures 5 and 6, respectively. The graphic of variation of drag coefficient with rate of rotation has bell shape. Maximum peak values of C_D occurs at $\alpha \approx -1.5$. The value of C_D has a maximum at smallest aspect ratio. The nonmonotonic behavior of C_D with rotation rate occurs due to variation of the pressure force as shown in Figure 6.

Figure 6 shows the pressure and viscous drag coefficient contribution to the total drag coefficient for the three aspect ratios at Re = 40. For all aspect ratios, the viscous contribution C_{D_f} slightly increase, when α changes from 2 to -4. Interestingly, for Ar = 2 at $\alpha \approx 1.6$, the viscous drag C_{D_f} decreases rapidly while the pressure drag C_{D_p} increases as the same rate and the total drag on the torus vanishes that correspond to the self-motion of the torus.

5. Conclusions

In the present study, we have investigated numerically the problem of the steady viscous incompressible fluid flow over a rotating torus for a range of the aspect ratios $2 \leq Ar \leq 5$, and a range of rotational rate, $-4.0 \leq \alpha \leq 2.0$. Rotation of surface in positive direction formed a vortex around the torus surface. The main stream flows around the rotating toroidal fluid region which encloses the rigid torus rotating around its centerline. Rotating surface in negative direction accelerate portion of the incoming stream passing through the hole and generates the jet of fluid expelled from
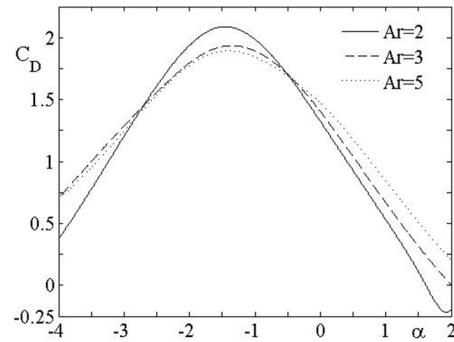

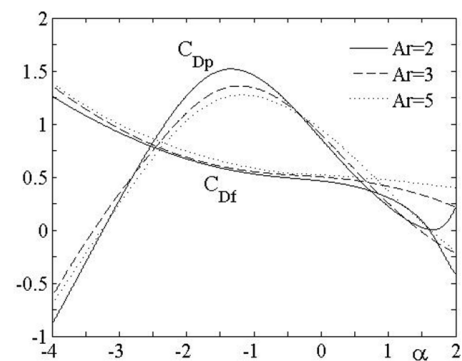Figure 5. Variation of drag coefficient with rate of rotation for aspect ratios Ar = 2, 3 and 5 at Re = 40.

Figure 6. Variation of pressure and viscous drag coefficients with rate of rotation for aspect ratios Ar = 2, 3 and 5 at Re = 40.

the hole downward.

The changes in the variation of the pressure and vorticity distributions are more serve on the inner surface of the torus, especially for a small aspect ratio Ar ≤ 2. For a positive rotation, C_D increases monotonically with increasing Ar but shows a nonmonotonic behavior at negative rotation. For a positive rotation, the total drag coefficient C_D decreases monotonically as α increases. However, in the case of negative rotation, C_D is no longer a monotonic function of α.

References

Ghosh, S. 1927. On the steady motion of a viscous liquid due to translation of a tore parallel to its axis. Bulletin of the Calcutta Mathematical Society. 18, 185-194.

Jonhson, R.E. and Wu, T.Y. 1979. Hydromechanics of low-Reynolds-number flow. Part 5. Motion of a slender torus. Journal of Fluid Mechanics. 96(2), 263-277.

Leshansky, A.M. and Kenneth, O. 2008. Surface tank treading: Propulsion of Purcell's toroidal swimmer. Physics of Fluids. 20, 063104.

Majumdar, S.R. and O'Neill, M.E. 1977. On axisymmetric Stokes flow pas a torus. Journal of Appilled Mathematics Physics. 28, 541-550.

Pell, W.H. and Payne, L.E. 1960. On Stokes flow about a torus. Mathematika. 7, 78-92.

Sheard, G.J., Thompson, M.C., and Hourigan, K. 2003. From spheres to circular cylinders: the stability and flow structures of bluff ring wakes. Journal of Fluid Mechanics. 492, 147-180.

Sheard, G.J., Hourigan, K., and Thompson, M.C. 2005. Computations of the drag coefficients for low-Reynolds-number flow past rings. Journal of Fluid Mechanics. 526, 257–275.

Thaokar, R.M., Schiessel, H., and Kulic, I.M. 2007. Hydrodynamics of a rotating torus. Euro Physics Journal B. 60, 325-336.

Yanenko, N.N. 1971. The method of Fractional Steps: The Solution of Problems of Mathematical Physics in Several Variables, Springer-Verlag, New York, U.S.A.